Hindawi Publishing Corporation
Journal of Nanotechnology
Volume 2016, Article ID 5375939, 7 pages
http://dx.doi.org/10.1155/2016/5375939

Research Article

Sol-Gel Titanium Dioxide Nanoparticles: Preparation and Structural Characterization

Oon Lee Kang,[1] Azizan Ahmad,[1] Usman Ali Rana,[2] and Nur Hasyareeda Hassan[1]

[1]*Faculty of Science and Technology, Universiti Kebangsaan Malaysia, 43600 Bangi, Selangor, Malaysia*
[2]*Sustainable Energy Technologies (SET) Center, King Saud University, P.O. Box 800, Riyadh 11421, Saudi Arabia*

Correspondence should be addressed to Nur Hasyareeda Hassan; syareeda@ukm.edu.my

Received 29 June 2016; Accepted 15 November 2016

Academic Editor: Paresh Chandra Ray

Titanium dioxide (TiO_2) nanoparticle was achieved in an alternative sol-gel route, as involved in 1 M acidic solution: HCl-tetrahydrofuran (HCl-THF), HNO_3-tetrahydrofuran (HNO_3-THF), and $ClHNO_2$-tetrahydrofuran ($ClHNO_2$-THF) solution. Resultant TiO_2 nanoparticle was further investigated in a systematic analytical approach. Nanoscale TiO_2 structure was observed at a moderate hydrolysis ratio ($8 \leq R_H \leq 16$). Particle size range was much narrower in an aprotic HNO_3-THF medium, as compared to a differential HCl-THF medium. Biphasic TiO_2 structure was detected at a certain hydrolysis ratio ($R_H \geq 16$). Even so, relative anatase content was rather insignificant in an aprotic HCl-THF medium, as compared to a differential HNO_3-THF medium. Tetragonal TiO_2 structure was observed in the entire hydrolysis ratio ($4 \leq R_H \leq 32$). Interstitial lattice defect was evident in an aprotic HNO_3-THF medium but absent in a differential $ClHNO_2$-THF medium.

1. Introduction

Titanium dioxide (TiO_2) nanoparticles are applicable to high performance technologies, as evident in current innovative applications [1]. TiO_2 nanoparticles are therefore considered as superior functional materials [2, 3]. Stoichiometric TiO_2 nanoparticles are categorized as active dielectric ($\kappa > 3.9$) materials; nonstoichiometric TiO_{2-x} nanoparticles are categorized as intrinsic semiconductor materials [4].

TiO_2 nanoparticles are proven effective in numerous optoelectronic applications. Such predominant phenomena are related to superior optoelectronic properties: high dielectric constant, high transmission coefficient, and high breakdown strength [5]. TiO_2 nanoparticles are also beneficial to several photovoltaic applications [6]. Such predominant phenomena are related to sufficient photoreactive properties [7].

TiO_2 nanoparticles are prevalent in three distinct metastable configurations: tetragonal, monoclinic, and orthorhombic [8]. In general, anatase TiO_2 nanostructures are more reactive than other polymorphic configurations. Such preferences are attributed to distinctive crystallographic properties [9]. Even so, anatase TiO_2 nanostructures are rather difficult to synthesize, as susceptible to phase transformation [10].

In the recent past, anatase TiO_2 nanostructures are often derived from sol-gel reaction [11]. Resultant internal nanostructures are more dependent on hydrolysis ratio. Spherical monodisperse nanostructures are achieved at stoichiometric ratio ($R_H = 4$). Resultant internal nanostructures are also dependent on hydrolysis catalyst [12, 13]. Dense microporous nanostructures are achieved in acidic catalysis ($R_H > 4$); loose mesoporous nanostructures are achieved in basic catalysis.

In the present investigation, TiO_2 nanoparticles were achieved in sol-gel synthesis: HCl-THF, HNO_3-THF, and $ClHNO_2$-THF catalysis. Resultant TiO_2 nanoparticles were then subjected to systematic characterization.

2. Methods

2.1. TiO_2 Nanoparticles Preparation. TiO_2 sol solutions were obtained at a specific H_2O/alkoxide molar ratio (Table 1). TiO_2 sol solutions were stirred at ambient room temperature (2 hours). Resultant sol particles were then dried in microwave oven.

Table 1: Hydrolysis molar ratio.

Metal alkoxide ($Ti_4(OCH_2CH_3)_{16}$)	Catalysts (HCl, HNO_3, and $ClHNO_2$)	Solvent (THF)	DDH_2O
1	1	4	4
1	1	4	8
1	1	4	16
1	1	4	32

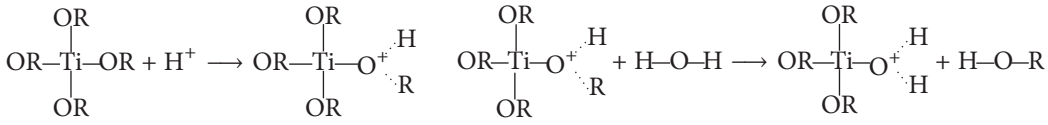

Scheme 1

2.2. TiO_2 Nanoparticles Characterization. DLS analyses were conducted on a Malvern Zetasizer Nano ZS DLS spectrometer (Malvern Instruments GmbH, Herrenberg, Germany). DLS data were acquired in the backscattered mode. DLS data were collected at a fixed detection angle ($\theta = 173^\circ$).

SEM analyses were conducted on a Carl Zeiss LEO 1450 VP microscope (Carl Zeiss AG, Oberkochen, Germany). SEM micrographs were acquired in the backscattered electron (BSE) mode. SEM micrographs were taken at a moderate acceleration voltage (15–20 kV).

XRD analyses were conducted on a Bruker D8 Advance diffractometer (Bruker AXS GmbH, Karlsruhe, Germany). XRD patterns were acquired in the symmetrical Bragg-Brentano configuration. XRD patterns were recorded in the 2-theta (θ) range (15–60°; step size 0.02°).

FTIR analyses were conducted on a Perkin-Elmer Spectrum 400 spectrometer (Perkin-Elmer Ltd, Buckinghamshire, UK). FTIR spectra were acquired in the attenuated total reflectance (ATR) mode. FTIR spectra were recorded in the mid-infrared range (4000–650 cm^{-1}; spectral resolution 4 cm^{-1}).

3. Results and Discussion

3.1. Particle Size Distribution and Morphological Characterization. Particle size data was presented in graphical form (histogram), as shown in Figure 1.

Broad particle size distribution was observed at high hydrolysis ratio ($R_H = 32$). Broad particle size distribution is attributed to rapid condensation reaction, as commenced before hydrolysis completion.

Particle growth process is accelerated at high condensation rate [14]. In such a case, particle growth process is pertained to monomers (Ti-OH) addition. Particle growth rate is dependent on interface reaction. In effect, rapid growth rate is expected at high monomers concentration. Dense aggregate structure ($D_f \approx 3.00$) is predominant in monomers addition.

Narrow particle size distribution was observed at moderate hydrolysis ratio ($8 \leq R_H \leq 16$). Narrow particle size distribution is attributed to more efficient hydrolysis reaction [15].

Distinct growth process is anticipated at high hydrolysis rate (Figure 2). More specific, particle growth process is pertained to clusters (Ti-OH-Ti) aggregation [16]. Particle growth rate is dependent on Brownian motion. In effect, rapid growth rate is expected at high effective collision. Fractal aggregate structure ($D_f \approx 2.09$) is predominant in clusters aggregation.

Broad particle size distribution was observed in HCl-THF medium. Broad particle size distribution is attributed to concurrent hydrolysis and condensation reactions. Such critical phenomenon is correlated to insignificant acidification.

Narrow particle size distribution was observed in HNO_3-THF medium. Narrow particle size distribution is attributed to sequential hydrolysis and condensation reactions. Such critical phenomenon is correlated to significant protonation.

Particle formation process is preferred in high acidic medium. In particular, S_N1 mechanism is involved in high acidic medium. Local equilibrium behavior is dependent on ionic strength gradient.

Metal alkoxide (Ti-OR) group is protonated in the initial step. In such a case, Ti-$OR^{+\bullet}$ species is susceptible to hydrolysis reaction (Scheme 1).

Reactive Ti-$OH^{+\bullet}$ species can react further in the subsequent step. Ti-O-Ti network structure is achieved in oxolation reaction; M-OH-M network structure is achieved in olation reaction (Scheme 2).

Smallest particle size data ($R_H = 16$) is subjected to SEM measurement. DLS particle size data is based on hydrodynamic parameter, and therefore, resultant particle size distribution is much broader than SEM result. Similar observation was also reported in several previous studies [17].

Small aggregate particles were discerned in uniform bright contrast. Each aggregate particle does not exceed 50 nm in size. Small aggregate particles are attributed to attractive interparticle interactions, electrostatic attractive force, and covalent interactive force.

3.2. Phase Identification. Diffraction pattern was presented in the 2-theta range ($15^\circ < 2\theta < 65^\circ$), as shown in Figure 3.

Broad diffraction hump was obtained at low hydrolysis ratio ($R_H \leq 8$). Broad diffraction hump was observed

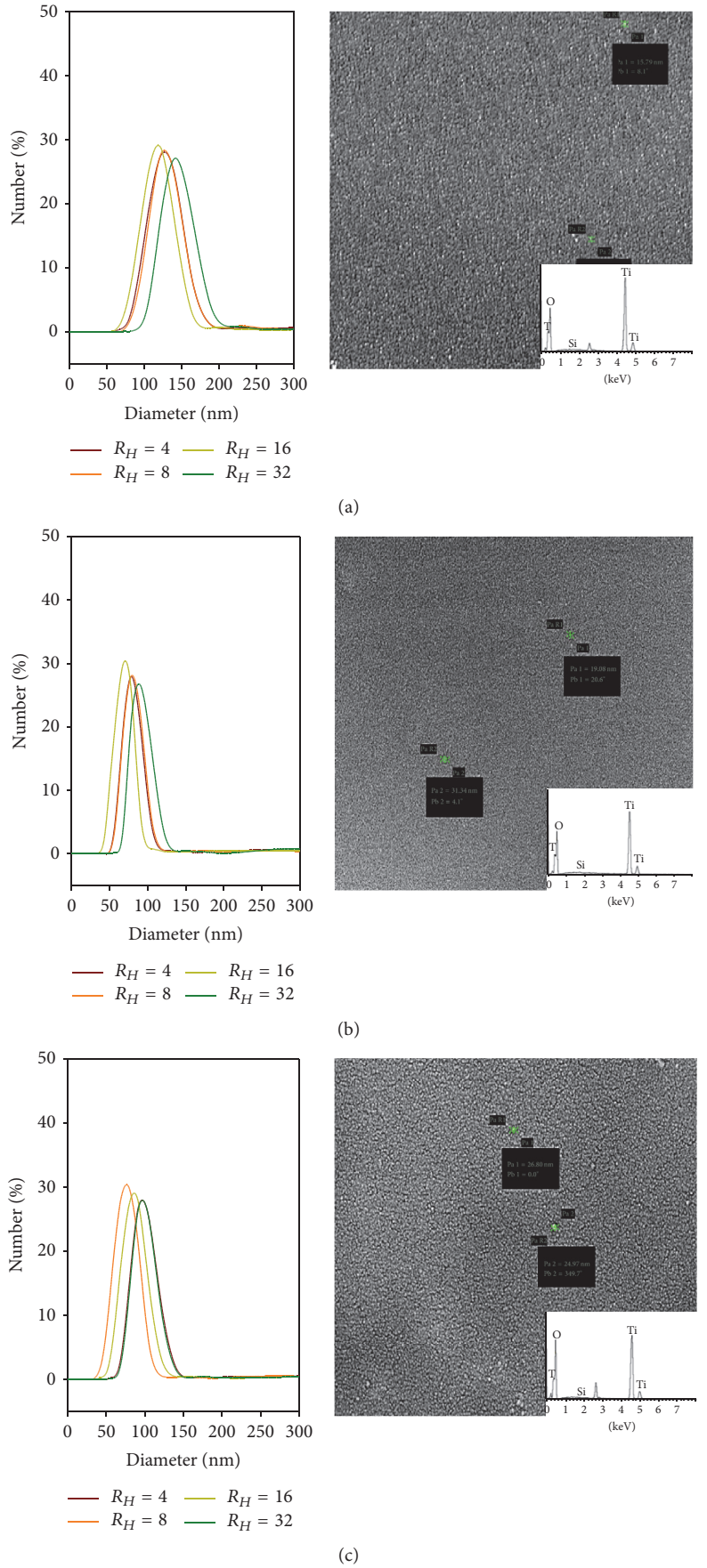

Figure 1: Particle size data and SEM micrograph: (a) HCl-THF/TiO_2, (b) HNO_3-THF/TiO_2, and (c) $ClHNO_2$-THF/TiO_2 nanoparticles.

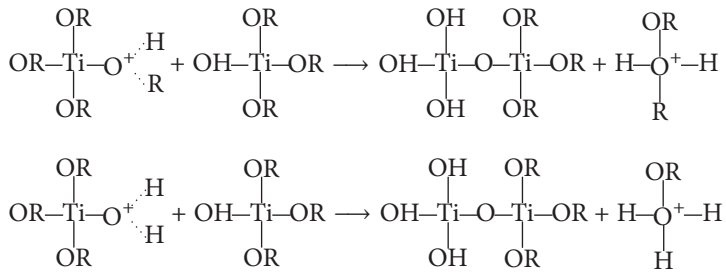

Scheme 2

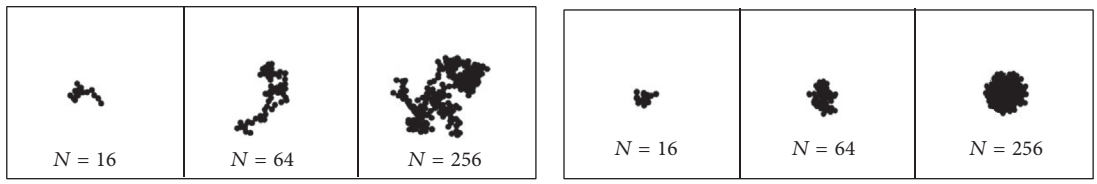

Figure 2: Particle growth mechanism: (a) clusters aggregation and (b) monomers addition.

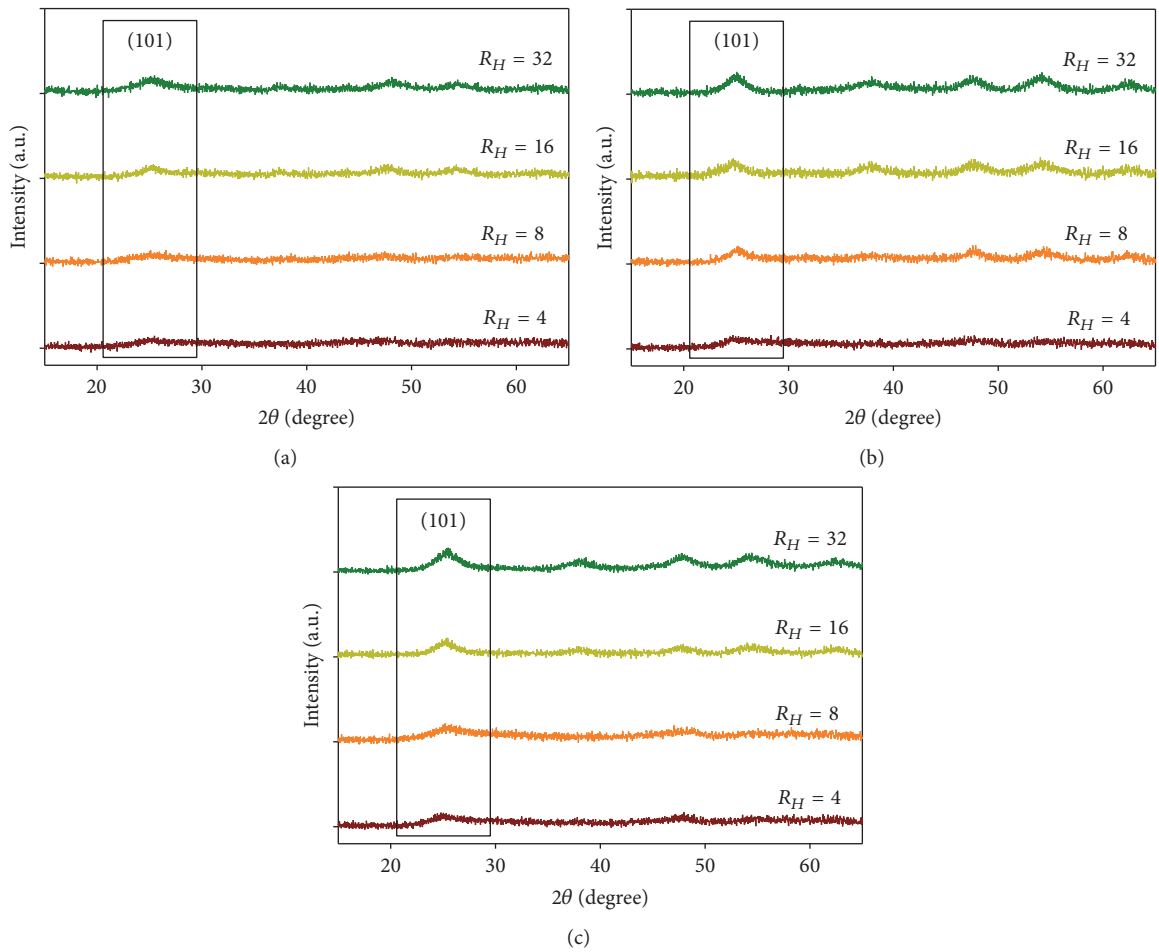

Figure 3: XRD diffraction patterns: (a) HCl-THF/TiO_2, (b) HNO_3-THF/TiO_2, and (c) $ClHNO_2$-THF/TiO_2 nanoparticles.

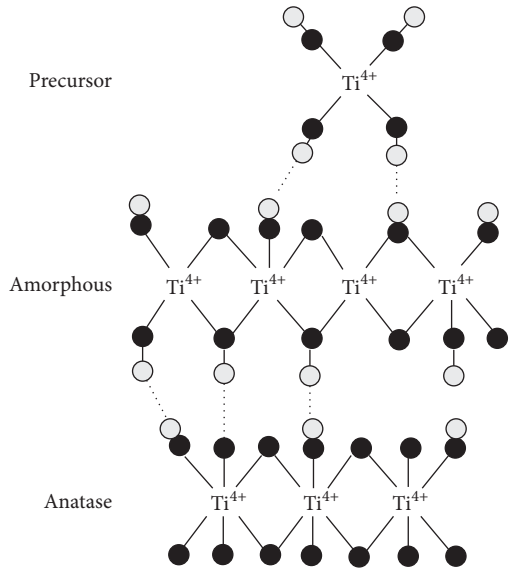

Figure 4: Titanium-oxygen (Ti-O) lattice rearrangement.

at $2\theta = 25.3^{\circ}$. Such diffraction hump is attributed to random lattice orientation. In this particular case, amorphous TiO_2 nanostructure is encountered in sixfold octahedral coordination but no fourfold tetrahedral coordination.

Broad intense diffraction band was observed at high hydrolysis ratio ($R_H \geq 16$). Preferable anatase diffraction band was detected at $2\theta = 25.3^{\circ}$ (101), 37.9° (004), 48.1° (200), 54.3° (105), and 62.5° (204).

More specific, anatase TiO_2 nanostructure is achieved in gradual titanium-oxygen lattice rearrangement, that is, Ti-O bonds disproportionation (Figure 4). In literature, anatase TiO_2 nanostructure is arranged in fourfold coordination: each Ti atom is linked to six oxygen atoms; each oxygen atom is linked to three Ti atoms [18].

Less intense diffraction band was obtained in HCl-THF medium. In such a case, phase transformation process is restricted in HCl-THF catalysis.

Broad intense diffraction band was obtained in HNO_3-THF medium. In such a case, phase transformation process is preferred in HNO_3-THF catalysis. Phase transformation process is mediated at low ambient supersaturation. Such critical phenomenon is attributed to rapid hydrolysis reaction.

Phase transformation process is spontaneous in aqueous acidic medium. Phase transformation process can occur in multiple distinct stages: nucleation, growth, and further coalescence [19]. Nucleation process is achieved in successive monomers condensation. Nucleation process is preferred above critical crystallite size, that is, 12 Ti-O bonds dimension. In general, nucleation rate is dependent on monomers concentration.

Crystallite growth process is achieved in monomers (Ti-OH) addition. Crystallite growth process is based on interface reaction, as involved in mass transfer (or heat transfer). In effect, crystallite growth rate is dependent on thermodynamic properties.

3.3. Structural Characterization. IR absorption spectrum was presented in the mid-infrared region (4000–650 cm^{-1}), as shown in Figure 5.

TiO_2 characteristic band was obtained in HCl-THF and $ClHNO_2$-THF medium. Ti-O absorption band was observed at 950 and 850 cm^{-1}. Such absorption band is assigned to tetrahedral $[TiO_4]^{4-}$ units. In such a case, Ti-O network structure is encountered in tetrahedral $[TiO_4]^{4-}$ coordination.

Ti-OH absorption band was observed at 3800–3750 cm^{-1}, but not obvious. In such a case, subsequent condensation reaction is continued till tetrahedral $[TiO_4]^{4-}$ formation.

Board hydroxyl absorption band was observed at 3600–3000 cm^{-1}. Broad absorption band is attributed to intermolecular interactions (e.g., $H_2O\cdots H_2O$ and/or $Ti\text{-}OH\cdots H_2O$ interactions) (Figure 6). In general, surface hydroxyl group is resided at octahedral surface. Surface hydroxyl group is beneficial in photocatalytic activities.

Surface H_2O absorption band was observed at 1620 cm^{-1}. Surface H_2O absorption process is beneficial to heat generation, as consequence in Ti^{4+}-OH_2 bonds formation. In effect, phase transformation process is possible in ambient operational condition.

N-TiO_2 characteristic band was obtained in observed in HNO_3-THF medium. Ti-O-N absorption band was observed at 1550, 1300, and 1050 cm^{-1}. Such absorption band is corresponded to interstitial nitrogen sites. In such a case, Ti-O-N network structure is encountered in interstitial coordination, rather than substitutional coordination (Figure 7).

Nitrate (NO_3) absorption band was observed at 1400 cm^{-1}. Nitrate anion is chelated in bidentate fashion, and therefore, nitrate anion is rather difficult to eliminate.

4. Conclusions

Resultant TiO_2 nanostructure was dependent on chemical reaction parameters. Narrower size range was obtained at a

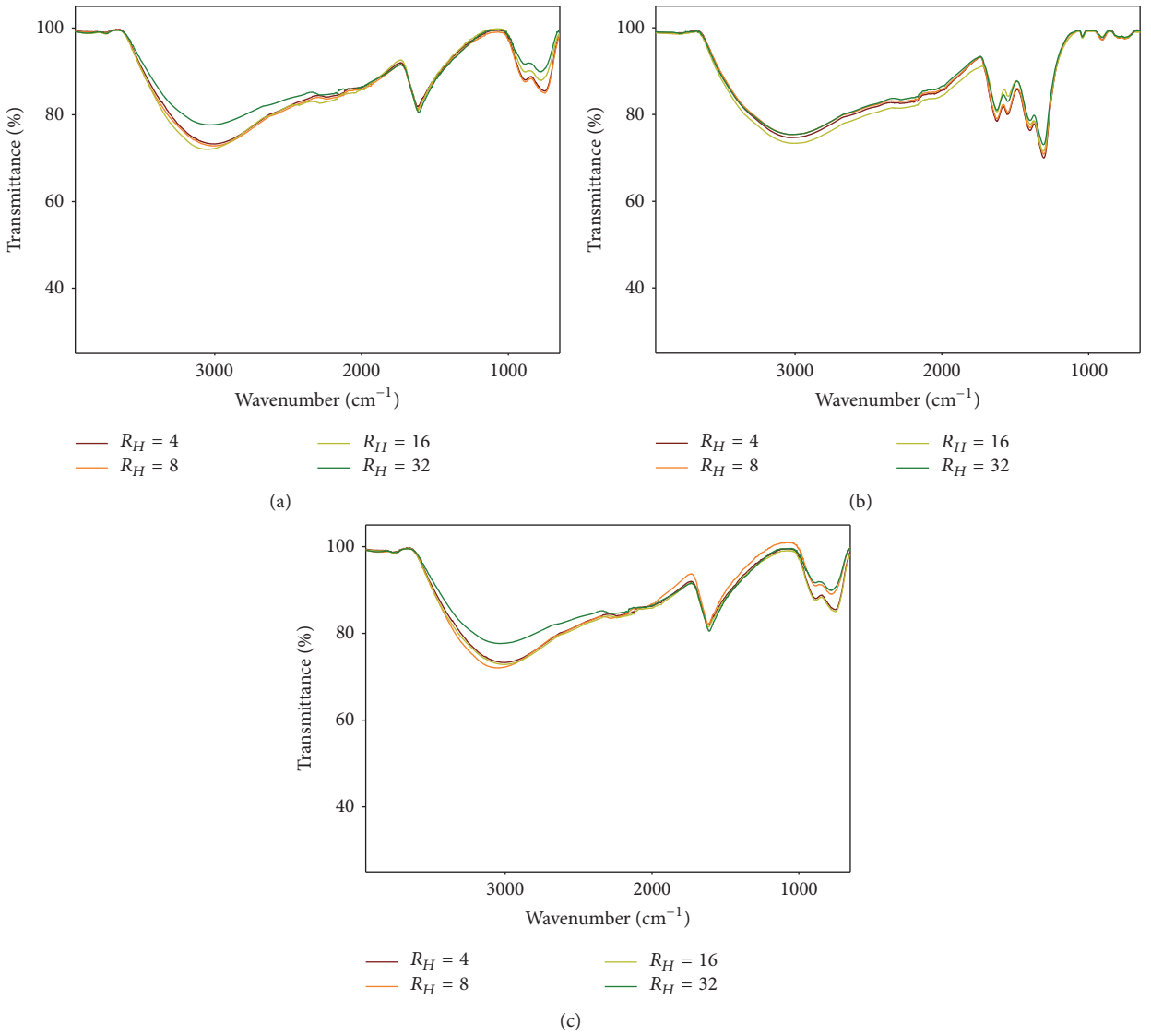

Figure 5: IR absorption spectra: (a) HCl-THF/TiO_2, (b) HNO_3-THF/TiO_2, and (c) $ClHNO_2$-THF/TiO_2 nanoparticles.

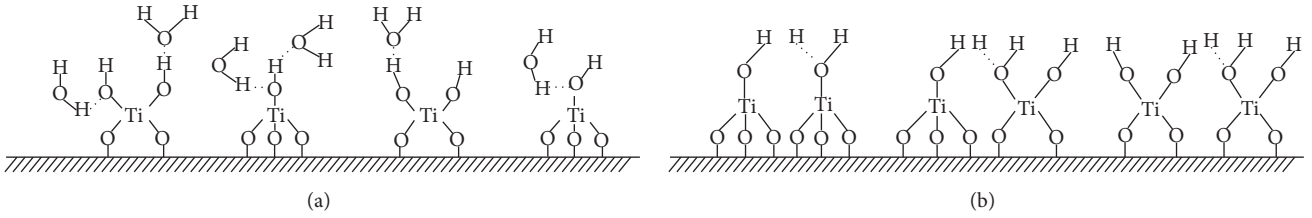

Figure 6: H-bonds formation mechanism: (a) Ti-OH$\cdots H_2O$ interaction and (b) Ti-OH$\cdots$HO-Ti interaction.

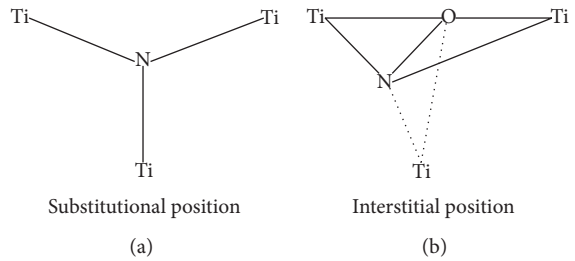

Figure 7: Ti-O-N network formation: (a) substitutional coordination and (b) interstitial coordination.

moderate hydrolysis ratio ($R_H = 16$). Substantial anatase phase was achieved in a certain hydrolysis ratio ($R_H \geq 16$). Even more, interstitial lattice defect was developed in an aprotic HNO_3-THF medium.

Competing Interests

The authors declare that they have no competing interests.

Acknowledgments

O. L. Kang would like to extend his sincere appreciation to Universiti Kebangsaan Malaysia for financial support through University Research Grants (1) NND/NM(2)/TD11-046, (2) ERGS/1/2013/TK07/UKM/02/4, and (3) FRGS/1/2014/ST01/UKM/02/1. O. L. Kang would also like to extend his sincere appreciation to the CRIM for technical support. U. A. Rana would like to extend his sincere appreciation to King Saud University for financial support through Prolific Research Group, Project no. PRG-1436-18.

References

[1] M. Sharon, F. Modi, and M. Sharon, "Titania based nanocomposites as a photocatalyst: a review," *AIMS Materials Science*, vol. 3, no. 3, pp. 1236–1254, 2016.

[2] J. Mech, K. Mech, and K. Szaciłowski, "TiO_2-anthraquinone hybrids: from quantum-chemical design to functional materials," *Journal of Materials Chemistry C*, vol. 3, no. 16, pp. 4148–4155, 2015.

[3] O. L. Kang, A. Ahmad, N. H. Hassan, and U. A. Rana, "[MG49-$LiClO_4$]:[TiO_2-SiO_2] polymer electrolytes: in situ preparation and characterization," *International Journal of Polymer Science*, vol. 2016, Article ID 9838067, 10 pages, 2016.

[4] A. Di Paola, M. Bellardita, and L. Palmisano, "Brookite, the least known TiO_2 photocatalyst," *Catalysts*, vol. 3, no. 1, pp. 36–73, 2013.

[5] T. A. Kandiel, A. Feldhoff, L. Robben, R. Dillert, and D. W. Bahnemann, "Tailored titanium dioxide nanomaterials: anatase nanoparticles and brookite nanorods as highly active photocatalysts," *Chemistry of Materials*, vol. 22, no. 6, pp. 2050–2060, 2010.

[6] B. Laskova, M. Zukalova, A. Zukal, M. Bousa, and L. Kavan, "Capacitive contribution to Li-storage in TiO_2 (B) and TiO_2 (anatase)," *Journal of Power Sources*, vol. 246, pp. 103–109, 2014.

[7] F. Fresno, R. Portela, S. Suárez, and J. M. Coronado, "Photocatalytic materials: recent achievements and near future trends," *Journal of Materials Chemistry A*, vol. 2, no. 9, pp. 2863–2884, 2014.

[8] K. Sabyrov, N. D. Burrows, and R. L. Penn, "Size-dependent anatase to rutile phase transformation and particle growth," *Chemistry of Materials*, vol. 25, no. 8, pp. 1408–1415, 2013.

[9] F. De Angelis, C. Di Valentin, S. Fantacci, A. Vittadini, and A. Selloni, "Theoretical studies on anatase and less common TiO_2 phases: bulk, surfaces, and nanomaterials," *Chemical Reviews*, vol. 114, no. 19, pp. 9708–9753, 2014.

[10] A. Fujishima, X. Zhang, and D. A. Tryk, "TiO_2 photocatalysis and related surface phenomena," *Surface Science Reports*, vol. 63, no. 12, pp. 515–582, 2008.

[11] E. Blanco, J. M. González-Leal, and M. Ramírez-del Solar, "Photocatalytic TiO_2 sol-gel thin films: optical and morphological characterization," *Solar Energy*, vol. 122, pp. 11–23, 2015.

[12] R. Ciriminna, A. Fidalgo, V. Pandarus, F. Béland, L. M. Ilharco, and M. Pagliaro, "The sol-gel route to advanced silica-based materials and recent applications," *Chemical Reviews*, vol. 113, no. 8, pp. 6592–6620, 2013.

[13] J. A. Van Hensbergen, M. Liu, R. P. Burford, and A. B. Lowe, "Simultaneous ROMP and titania sol-gel reactions and nanodispersed functional organic-inorganic composite hybrid materials," *Journal of Materials Chemistry C*, vol. 3, no. 3, pp. 693–702, 2015.

[14] M. K. Patil, S. Shaikh, and G. Ibram, "Recent advances on TiO_2 thin film based photocatalytic applications (a review)," *Current Nanoscience*, vol. 11, no. 3, pp. 271–285, 2015.

[15] S. Laurent, D. Forge, M. Port et al., "Magnetic iron oxide nanoparticles: synthesis, stabilization, vectorization, physicochemical characterizations and biological applications," *Chemical Reviews*, vol. 108, no. 6, pp. 2064–2110, 2008.

[16] S. Babu, M. Rottereau, T. Nicolai, J. C. Gimel, and D. Durand, "Flocculation and percolation in reversible cluster-cluster aggregation," *European Physical Journal E*, vol. 19, no. 2, pp. 203–211, 2006.

[17] R. Raliya, P. Biswas, and J. C. Tarafdar, "TiO_2 nanoparticle biosynthesis and its physiological effect on mung bean (*Vigna radiata* L.)," *Biotechnology Reports*, vol. 5, no. 1, pp. 22–26, 2015.

[18] P. Giesz, G. Celichowski, D. Puchowicz et al., "Microwave-assisted TiO_2: anatase formation on cotton and viscose fabric surfaces," *Cellulose*, vol. 23, no. 3, pp. 2143–2159, 2016.

[19] B. Gilbert, H. Zhang, F. Huang, M. P. Finnegan, G. A. Waychunas, and J. F. Banfield, "Special phase transformation and crystal growth pathways observed in nanoparticles," *Geochemical Transactions*, vol. 4, pp. 20–27, 2003.